Quaternary Science Advances 2 (2020) 100012

Contents lists available at ScienceDirect

Quaternary Science Advances

journal homepage: www.journals.elsevier.com/quaternary-science-advances

Build-up and chronology of blue ice moraines in Queen Maud Land, Antarctica

Naki Akçar [a,b,*], Serdar Yeşilyurt [a,c], Kristina Hippe [d], Marcus Christl [d], Christof Vockenhuber [d], Vural Yavuz [e], Burcu Özsoy [b,f]

[a] Institute of Geological Sciences, University of Bern, Baltzerstrasse 1-3, 3012, Bern, Switzerland
[b] Polar Research Institute, TÜBITAK Marmara Research Center, Gebze, Istanbul, Turkey
[c] Department of Geography, Ankara University, Sıhhiye, 06100, Ankara, Turkey
[d] Laboratory of Ion Beam Physics (LIP), ETH Zurich, Otto-Stern-Weg 5, 8093, Zurich, Switzerland
[e] Faculty of Engineering, Turkish-German University, 34820, Beykoz, Istanbul, Turkey
[f] Maritime Faculty, Istanbul Technical University Tuzla Campus, Istanbul, Turkey

ARTICLE INFO

Keywords:
Blue ice moraine
Surface exposure dating
Cosmogenic nuclide
Inheritance
Sør rondane

ABSTRACT

Blue ice moraines are common supraglacial landforms in Antarctica and they are considered to record the ice volume fluctuations. In this study, we use photogrammetry and the analysis of multiple cosmogenic nuclides (^{10}Be, ^{26}Al, and in-situ ^{14}C) in boulders on three blue ice moraines to explore the timing of ice volume fluctuations in the Sør Rondane Mountains, Queen Maud Land, and provide insights into the role of sediment sources in the reconstruction of their chronology. In the field, we observe that the blue ice moraines are composed of subglacially and supraglacially transported sediments. Cosmogenic ^{10}Be and ^{26}Al exposure ages of 14 surface samples, collected from boulders on three blue ice moraines, range from 15.4 ± 1.1 to 659.5 ± 33.9 ka. ^{26}Al/^{10}Be ratios vary between 3.53 ± 0.20 and 7.01 ± 0.32, and many of these ratios indicate complex exposure histories. In contrast, among nine in-situ ^{14}C exposure ages, five vary between 4.2 ± 0.1 and 22.0 ± 1.3 ka, and four are saturated. We conclude that the accumulation of these blue ice moraines commenced before or during the global Last Glacial Maximum. Our results indicate that surficial sediment sources can yield exposure ages that are older than real exposure age, and exhibit a wider scatter. This can alter the reconstructed chronology of these landforms. The analysis of in-situ ^{14}C has a high potential in tracking the pace of their evolution, especially since the Last Glacial Maximum.

1. Introduction

Supraglacial sediment accumulations from the subsurface and/or locally from slope processes and meteorite falls in blue ice areas of Antarctica are attributed to blue ice moraines. In fact, these can be considered as medial moraines made of unconsolidated glacial debris trapped between two ice masses. Blue ice moraines can be of any shape depending on the balance of these masses. Their surface area varies from a few square meters to one hundred square kilometers (Kassab et al., 2019, and references therein), and these can either be linked to a nunatak or disconnected from it. Blue ice moraines are generally thought to be composed of subglacial sediments transported to the surface by the sublimation of ice (Corti et al., 2008; Sinisalo and Moore, 2010). Those linked to a nunatak, however, can contain additional supraglacial sediments deriving from the nunatak itself, such as slope debris captured gradually by the ice and/or a direct deposition on the ice by rock fall or avalanches.

Blue ice moraines store information about long-term variations in the ice mass and sediment transport in basal or deep ice (Jonsson, 1990) because they are direct products of sublimation and indicate a negative shift in the surface mass balance (Bintanja, 1999). They not only record changes in ice sheet dynamics, but also serve as traps for micrometeorites (e.g., Whillans and Cassidy, 1983; Genge et al., 2018) and as a habitat for microbial activity (e.g., Tytgat et al., 2016). The mechanism of their structure and evolution has not yet been completely understood. In addition, knowledge about their chronology is not just scarce because of a limited number of investigations but apparently absent. Their state-of-the-art exposure history based on cosmogenic nuclide analysis

* Corresponding author. Institute of Geological Sciences, University of Bern, Baltzerstrasse 1-3, 3012, Bern, Switzerland.
E-mail address: akcar@geo.unibe.ch (N. Akçar).

https://doi.org/10.1016/j.qsa.2020.100012
Received 2 March 2020; Received in revised form 29 May 2020; Accepted 15 June 2020
Available online 20 June 2020

spans a few thousand years to a few hundred thousand years (Altmaier et al., 2010; Fogwill et al., 2012; Suganuma et al., 2014; Hein et al., 2016; Kaplan et al., 2017).

To investigate the competence of in-situ cosmogenic nuclides in calibrating the timing of events in the formation of blue ice moraines and explore the potential effects of the sediment source on the reconstruction of their chronology, we focus on the blue ice moraines in the vicinity of the Princess Elisabeth Station in the Sør Rondane Mountains in Queen Maud Land in Antarctica (Fig. 1). We select three blue ice moraine sites according to the source of the sediments, and study them in detail. These sources are the subsurface, the slopes of the local nunataks, and the tributary cirques. The first site is an arcuate-shaped medial moraine made of monolithologic sediments originating from the local nunatak. The second site is a junction of two medial moraines, one fed by the main ice stream and the other by the tributary cirque. The third site is an arcuate-shaped terminal moraine without a linkage to local nunataks. We reconstruct the digital elevation models (DEM) of these sites with an unmanned aerial vehicle (UAV) and investigate their geomorphology in detail. For sampling, we focus on the geologically oldest or youngest crests in the blue ice moraines based on the detailed geomorphology. We follow the regular sampling strategy for surface exposure dating (e.g., Dunai, 2010), and sample 10 boulders and 4 cobbles for the analysis of cosmogenic ^{10}Be, ^{26}Al, and in-situ ^{14}C to reconstruct their chronology. The determination of the origin of the samples, either from the subsurface or the surface, was not possible because any physical or lithological evidence is absent in the field. In this study, we present the first in-situ ^{14}C data from blue ice moraines. We reconstruct a younger in-situ ^{14}C chronology with respect to the cosmogenic ^{10}Be and ^{26}Al chronology. We find that simple, or close to simple exposure histories of cosmogenic ^{10}Be and ^{26}Al may conceal the moraines' timing of their accumulation and evolution, thus potentially leading to misinterpretations. Therefore, we conclude that cosmogenic in-situ ^{14}C is essential in – and has a high potential for – revealing at least the most recent exposure history of the blue ice moraines. We also discuss the impacts of the sediment source on the cosmogenic nuclide accumulation.

2. Existing chronology of the blue ice moraines

Only a few of the blue ice moraines in Queen Maud Land have already been studied and their exposure dated. We recalculate exposure ages and ^{26}Al/^{10}Be ratios from the published literature with the online exposure age calculator formerly known as the CRONUS-Earth online calculator (http://hess.ess.washington.edu/math; Balco et al., 2008; cf. chapter 3.3 for the details). Suganuma et al. (2014) explored the Lunckeryggen blue ice moraine, which is deposited on the right lateral side of the Jennings Glacier in the Sør Rondane Mountains. The authors analyzed cosmogenic ^{10}Be in six boulders from different ridges in the moraine. Four boulders from the inner ridges (i.e., geologically younger) indicated recalculated exposure ages between 3 and 15 ka. Two boulders from the outer ridges yielded exposure ages of around 80 and 150 ka. Suganuma et al. (2014)

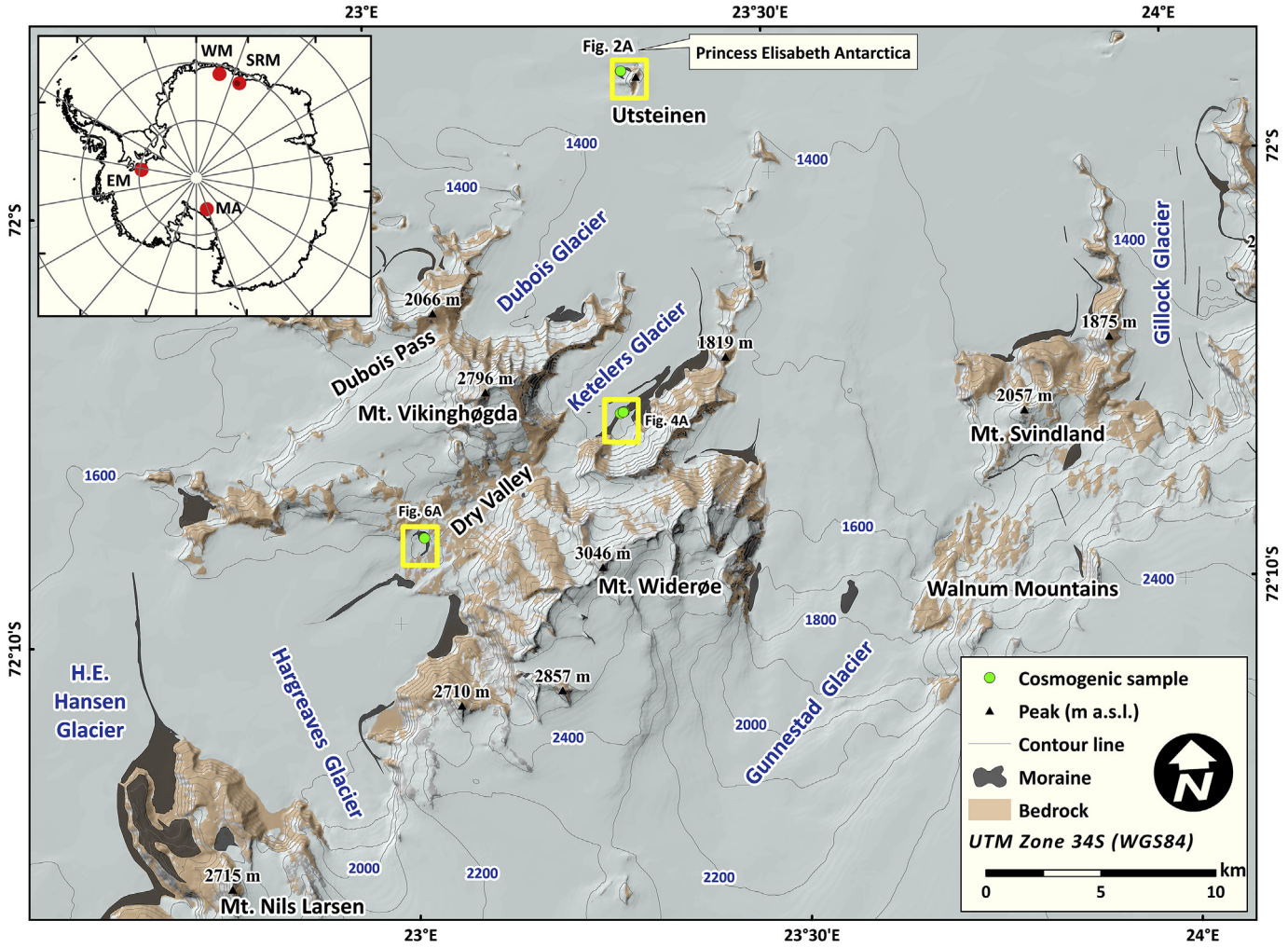

Fig. 1. Geographical map of the western Sør Rondane Mountains and locations of the study sites. Yellow rectangles show the extent of the maps given in the Figs. 2A, 4A and 6A. Moraines including the blue ice moraines in this region are also indicated. SRM: Sør Rondane Mountains; WM: Wohlthat Mountains; MA: Mount Achenar; EM: Ellsworth Mountains. Geospatial Information Authority of Japan (2014).

also studied the weathering characteristics of the sediments in the blue ice moraine after Moriwaki et al. (1991, 1994) and attributed it to Weathering Stage 1 based on the low weathering index values, meaning that the glacial deposits were largely intact. The clasts in this stage were fresh or relatively fresh with preserved glacial polish and striation, and with no or little iron staining. Based on cosmogenic nuclide analysis and weathering characteristics, the authors considered the Lunckeryggen blue ice moraine to have been built during the Late Pleistocene – Holocene.

Altmaier et al. (2010) investigated the Schüssel blue ice moraine in the Wohlthat Mountains in the Queen Maud Land. This moraine was deposited by one of the tongues of the Lednik Gornogo Instituta Glacier. The authors analyzed 13 rock surfaces along this blue ice moraine. Recalculated exposure ^{10}Be ages of 10 boulders varied between 7 ka and 1 Ma. The authors additionally analyzed ^{26}Al in three samples, which yielded ^{26}Al/^{10}Be ratios of 4.26 ± 0.24, 5.07 ± 0.53, and 5.07 ± 0.94 (recalculated), indicating complex exposure histories. While excluding the oldest exposure age, Altmaier et al. (2010) concluded that the formation of the Schüssel blue ice moraine started at around 120 ka and continued until around less than 5 ka as a result of the accumulation of debris entrained at the wet-based/ground-based boundary of the glacier (Altmaier et al., 2010).

Blue ice moraines were also studied elsewhere in the Antarctic mountains. The Mount Achenar blue ice moraine of the Law Glacier in the central Transantarctic Mountains is most probably the most intensively studied blue ice moraine in Antarctica (Kassab et al., 2019, and references therein). Cosmogenic ^{3}He, ^{10}Be, and ^{26}Al analysis from boulder surfaces along a transect in the Mount Achenar blue ice moraine indicated a continuous accumulation of debris during the last 300 ka, at least (Hagen, 1995; Kaplan et al., 2017). The measured ^{26}Al/^{10}Be ratios indicated a relatively simple exposure history (*sensu lato*), which means that the analyzed boulders did not experience burial periods longer than 100 ka (Kaplan et al., 2017). Based on the existing chronology, Graly et al. (2018) identified three chronozones in the same blue ice moraine: Pre-Last Glacial Maximum, Last Glacial Maximum (LGM), and Holocene. Based on seismic analysis and cosmogenic nuclide chronology, Kassab et al. (2019) proposed accretion rates ranging from 0.25 cm/ka to 0.43 cm/ka for the moraine.

Another well-studied example are the blue ice moraines in the Ellsworth Mountains in the Heritage Range (Fogwill et al., 2012; Hein et al., 2016; Sugden et al., 2017). The studies in this region focused on the blue ice moraines in the Patriot, Independence, and Marble Hills. In the Patriot Hills blue ice moraine, 11 ^{10}Be, 3 ^{26}Al, and 1 ^{21}Ne cosmogenic exposure ages were provided. ^{10}Be exposure ages varied between 0.1 and 87 ka, and one of three ^{26}Al/^{10}Be ratios indicated a simple exposure history with a ratio of 7.07 ± 1.28 (recalculated). This simple exposure history yielded an exposure age of 1.4 ka $\pm$ 0.2 ka (recalculated). However, one ^{10}Be/^{21}Ne ratio showed a more complex exposure history. In the Independence Hills blue ice moraine, four erratic boulders and four erratic cobbles (two of them were limestones) were analyzed, of which 6 determined cosmogenic ^{10}Be exposure ages ranged from 1.2 to 40 ka. One ^{26}Al/^{10}Be ratio of 8.2 ± 0.4 showed a simple exposure of 40 ka. Two ^{36}Cl exposure ages were 19 and 35 ka (Hein et al., 2016). Seven ^{10}Be exposure ages from the Marble Hills blue ice moraine yielded an exposure shorter than 3 ka (Fogwill et al., 2012; Hein et al., 2016; Sugden et al., 2017). One of the two measured ^{26}Al/^{10}Be ratios showed close to simple exposure with a ratio of 5.08 ± 1.24 (recalculated). The other yielded an extremely high ^{26}Al/^{10}Be ratio (63 ± 537; recalculated). However, one ^{10}Be/^{21}Ne ratio also displayed a complex exposure. Based on these results, Fogwill et al. (2012) concluded that the accumulation of the blue ice moraines might have taken many tens of thousands of years. This conclusion is in agreement with suggestions the meteorite studies from finds in blue ice fields in Antarctica (e.g., Fireman et al., 1979; Herzog et al., 2015; Zekollari, 2019), as well as oxygen isotope studies (e.g., Faure et al., 1992; Korotkikh et al., 2011; Graly et al., 2018).

3. Materials and methods

3.1. Study area

The Sør Rondane Mountains in Queen Maud Land in East Antarctica are composed of several nunataks. These outcrop in an area of ~2000 km^2. The highest peak is Mount Widerøe at 3046 m above sea level (a.s.l.) (Fig. 1). The nunataks are lying in a metamorphic terrain, which has been geologically stable at least since the Late Cambrian as active tectonic structures and Cenozoic volcanism are missing (Shiraishi et al., 1997; Suganuma et al., 2014). The nunataks in the western Sør Rondane Mountains are made of Late Proterozoic Amphibolite-facies and lower-grade metamorphic rocks intruded by Paleozoic granites and pegmatites, and partially covered by tills, except for the Dubois Pass, which consists of granulite facies metamorphic rocks (Shiraishi et al., 1997).

At present, the Sør Rondane Mountains act as a barrier to the ice in the south. This is displayed by the difference in altitude of the ice surface to the south and north of the mountain chain. To the south, the ice surface reaches >2500 m a.s.l. and forms an ice plateau. Lowlands of ice are found at altitudes of ~1500 m a.s.l. to the north of the mountain chain. Huge ice streams, such as the H.E. Hansen, Ketelers, and Gunnestad glaciers among others, actively drain the ice from the plateau to the lowlands (Fretwell et al., 2013; Mouginot et al., 2017; Rignot et al., 2017). During our field campaign within the BELARE 2017–2018 Expedition, we studied the Utsteinen, Ketelers and Dry Valley blue ice moraines in the Sør Rondane Mountains (Fig. 1).

3.2. Photogrammetry

To produce high resolution digital elevation models (DEM) of the blue ice moraines, we employed an unmanned aerial vehicle (DJI Mavick Pro©) to take aerial photographs. We planned the flight missions in Litchi Mission Hub® (https://flylitchi.com/hub). The flight altitude was 500 m above ground and the spacing between two flight lines was ~250 m (60–70% side overlap). The camera was set at an orthogonal position, and nadir images were captured automatically in a 7 s time interval to assure an 80% forward overlap. For a successful coverage of the studied landforms, we accomplished several flight missions per site. The missions covered a distance of ~9 km and took ~16–18 min, depending on the wind speed at the site. The aerial photographs were then processed by the photogrammetry software Agisoft Metashape®. In this way, we achieved ~17 cm/pixel cell size resolution orthoimages and DEMs of the study sites.

3.3. Cosmogenic nuclide analysis

We took 11 samples from the boulder top surfaces from the Ketelers and Dry blue ice moraines with a hammer and chisel, following the strategies presented in previous studies (e.g., Akçar et al., 2011). The sampled boulders were from 0.1 to 2.2 m above the surrounding ground. Lithology, geographical position, dimensions of the sampled boulders and cobble, sample thicknesses, and shielding correction factors are given in Table 1. In the Utsteinen blue ice moraine, we collected three gneiss slabs from the 20 cm high narrow crest deposited on the blue ice moraine (Figs. 2 and 3). To avoid any effect of post-depositional movement, we selected flat-lying, large and thin (<5 cm) slabs along the crest line. The thicknesses of these slabs were 3.5, 4.0, and 4.5 cm. In the light colored part of the Ketelers blue ice moraine, i.e., on the highest and outermost ridge of the main ice stream deposits, we sampled three boulders (KETEL-1, 2, and 3) (Fig. 4). Similarly, we collected three rock surface samples (KETEL-4, 5, and 6) from the highest and outermost ridge of the dark colored terminal moraine (Figs. 4 and 5). Thicknesses of the samples collected from the Ketelers blue ice moraine varied between 3.0 and 4.5 cm (Table 1). We collected surface samples from four boulders on the Dry blue ice moraine (DRY-1, 2, 3, and 4; Figs. 6 and 7). In

Table 1
Sample information from the Sør Rondane Mountains, Antarctica.

Sample Name	Lithology	Latitude, °N (DD.DD)	Longitude, °E (DD.DD)	Altitude (m a.s.l.)	Boulder Length (cm)	Boulder Width (cm)	Boulder Height (cm)	Sample Thickness (cm)	Shielding Factor[a]
UTSTE-1	Pegmatite	−71.95754	23.32147	1336	24	18	3.5	3.5	0.99342
UTSTE-2	Pegmatite	−71.95751	23.32158	1334	26	16	4.5	4.5	0.99342
UTSTE-3	Pegmatite	−71.95747	23.32173	1333	19	16	4.0	4.0	0.99342
KETEL-1	Granite	−72.09045	23.29667	1395	400	300	220	3.0	0.99676
KETEL-2	Metatonalite	−72.09029	23.29703	1401	300	300	100	4.0	0.99676
KETEL-3	Granite	−72.09065	23.29484	1403	250	140	100	4.5	0.99676
KETEL-4	Granite	−72.09001	23.30016	1396	400	200	120	4.0	0.99607
KETEL-5	Metatonalite	−72.09022	23.29906	1401	110	110	80	4.0	0.99607
KETEL-6	Metatonalite	−72.09024	23.29906	1394	200	150	80	4.0	0.99607
DRY-1	Granite	−72.13384	23.03574	1602	230	120	70	4.0	0.99751
DRY-2	Gneiss	−72.13400	23.03664	1607	330	200	140	5.0	0.99751
DRY-3	Gneiss	−72.13418	23.63691	1594	230	130	70	2.5	0.99751
DRY-4	Gneiss	−72.13429	23.63710	1596	140	120	80	4.0	0.99751
DRY-5	Metatonalite	−72.13429	23.63710	1596	30	30	10	5.0	0.99751

[a] Calculated for topographic shielding and dip of the surface after Dunne et al. (1999) with Matlab® Code provided by Tikhomirov et al. (2014) using mean attenuation length of 160 g/cm^2.

addition, we sampled an erratic cobble (DRY-5), which was deposited on the sampled gneiss boulder DRY-4. These samples were between 2.5 and 5 cm thick (Table 1).

We applied the modified version of the technique introduced by Kohl and Nishiizumi (1992) to separate and purify the quartz from the collected samples (Akçar et al., 2017). We extracted cosmogenic ^{10}Be and ^{26}Al for accelerator mass spectrometer (AMS) analysis at the ETH Zurich (Christl et al., 2013; Kubik and Christl, 2010) following the lab protocol described in Akçar et al. (2012) at the Surface Exposure Laboratory of the Institute of Geological Sciences at the University of Bern. We processed the samples in batches of nine samples and one full process blank. We measured ^{10}Be/^{9}Be and ^{26}Al/^{27}Al ratios at the 0.5 MV TANDY facility in Zurich. Then, we corrected the measured ^{10}Be/^{9}Be ratios using a long-term weighted average full process blank ratio of $(2.37 \pm 0.62) \times 10^{-15}$. We determined the total Al concentrations of the samples by inductively coupled plasma optical emission spectrometry (ICP-OES) at the Institute of Geological Sciences of the University of Bern. We calculated the ^{26}Al/^{10}Be ratios of the analyzed samples and those from previous studies mentioned in the text using the CRONUS-Earth exposure age calculator, and referenced them to 07KNSTD (Balco et al., 2008, and the update from v. 2.2 to v. 2.3 published by Balco in June 2016; .http://hess.ess.washington.edu/math/v.2.3). We then plotted the ^{26}Al/^{10}Be ratios versus ^{10}Be concentrations in a two-nuclide diagram (banana plot) using the iceTEA tool (http://ice-tea.org) and the MATLAB® code provided by Jones et al. (2019), with the time dependent Lal (1991)/Stone (2000) scaling model.

We performed in situ ^{14}C extraction with the new extraction system at the ETH Zurich (Lupker et al., 2019). We pre-heated around 4 g aliquots of the purified quartz for 2 h at 500 °C to remove atmospheric contaminations from the quartz surface, then heated for 3 h at 1670 °C to extract in-situ ^{14}C (Hippe, 2017). We then measured the ^{14}C/^{12}C ratio at the MICADAS facility in Zurich using a gas ion source (Ruff et al., 2007; Synal et al., 2007; Wacker et al., 2010). We measured the UTSTE samples and DRY-3 in December 2018 and March 2019, and the rest of the samples in Autumn and Winter 2019, therefore, we used different values for the blank correction and calculated the final ^{14}C concentrations following the protocol of Hippe and Lifton (2014) after subtracting a long-term processing blank of $(2.66 \pm 1.03) \times 10^4$ ^{14}C atoms (±1 st dev, n = 28) for the UTSTE samples and DRY-3, and of $(5.73 \pm 0.58) \times 10^4$ ^{14}C atoms (±1 st dev, n = 5) for the rest of the samples.

We computed cosmogenic ^{10}Be, ^{26}Al, and in-situ ^{14}C exposure ages, including the ones from previous studies mentioned in the text (input data taken from the Ice-D Antarctica Webpage http://hess.ess.washington.edu/iced/map/) with the online exposure age calculator formerly known as the CRONUS-Earth online calculator (http://hess.ess.washington.edu/math/v3/v3_age_in.html; Balco et al., 2008). We locally scaled the production rates of cosmogenic nuclides according to the time dependent Lal (1991)/Stone (2000) scaling scheme. We applied half-lives of 1.39 Ma (Chmeleff et al., 2010; Korschinek et al., 2010) for ^{10}Be, 0.71 Ma (Nishiizumi, 2004; Norris et al., 1983) for ^{26}Al, and 5700 years (www.nndc.bnl.gov) for ^{14}C in the age calculations. In the calculation of exposure ages, we accounted for topographic shielding (based on Dunne et al., 1999), sample thickness (using an exponential attenuation length of 160 g/cm^2), and rock density (2.65 g/cm^3). However, we did not correct the exposure ages for erosion and snow cover. The sample thickness and shielding correction factors are provided in Table 1.

4. Results

The cosmogenic nuclide data presented in Table 2 include the amount of dissolved quartz, the ^{9}Be spike, ^{10}Be concentration, total Al concentration, ^{26}Al concentration, and ^{26}Al/^{10}Be ratio. The amount of quartz used for in-situ ^{14}C analysis, CO_2 yield, modern ^{14}C fraction, δ^{13}C portion, ^{14}C/$^{12}C_{abs}$ ratio, the blank concentration used for the correction and the in-situ ^{14}C concentration are provided in Table 3.

The measured ^{10}Be concentrations ranged between $(0.40 \pm 0.01) \times 10^6$ and $(12.29 \pm 0.53) \times 10^6$ atoms/g, the ^{26}Al concentrations between $(1.99 \pm 0.14) \times 10^6$ and $(43.44 \pm 1.53) \times 10^6$ atoms/g, and the in-situ ^{14}C concentrations between $(18.57 \pm 0.33) \times 10^4$ and $(69.10 \pm 0.52) \times 10^4$ atoms/g. The currents of the samples KETEL-3 (for ^{10}Be) and DRY-4 (for ^{26}Al) were too low, not yielding enough for an acceptable AMS analysis. The total Al concentrations varied from 0.52 to 43.06 mg, and ^{26}Al/^{10}Be ratios from 3.53 ± 0.20 to 7.01 ± 0.32. The cosmogenic nuclide exposure and calculated landform ages are shown in Table 4. The calculated ^{10}Be exposure ages ranged from 18.2 ± 0.6 to 659.5 ± 33.9 ka, and those of ^{26}Al ranged from 16.5 ± 0.7 to 348.2 ± 5.8 ka. Four rock surface samples yielded saturation for in-situ ^{14}C and five samples had exposure ages from 4.2 ± 0.1 to 22.0 ± 1.3 ka.

4.1. Geomorphology and chronology of blue ice moraines

The Utsteinen blue ice moraine is an arcuate-shaped medial moraine wedged between the ice flowing from the Utsteinen cirque towards the northwest (Fig. 2A-C). It is monolithologic and composed of pebble-to boulder-sized pegmatite clasts. It displays dead-ice and permafrost features. This moraine is around 1 km long and ca. 50 m wide on average (Fig. 2D). It reaches a maximum width of around 90 m on its northern side (Fig. 2A). Its crest line is around 15 m above the blue ice on the outer side, and around 6 m above the blue ice on the inner side. We identified several decameter-high narrow crests, which show maximum positions of the ice from the Utsteinen cirque. ^{10}Be and ^{26}Al exposure ages of the slabs from these moraines range between 65 and 115 ka (Table 4). The

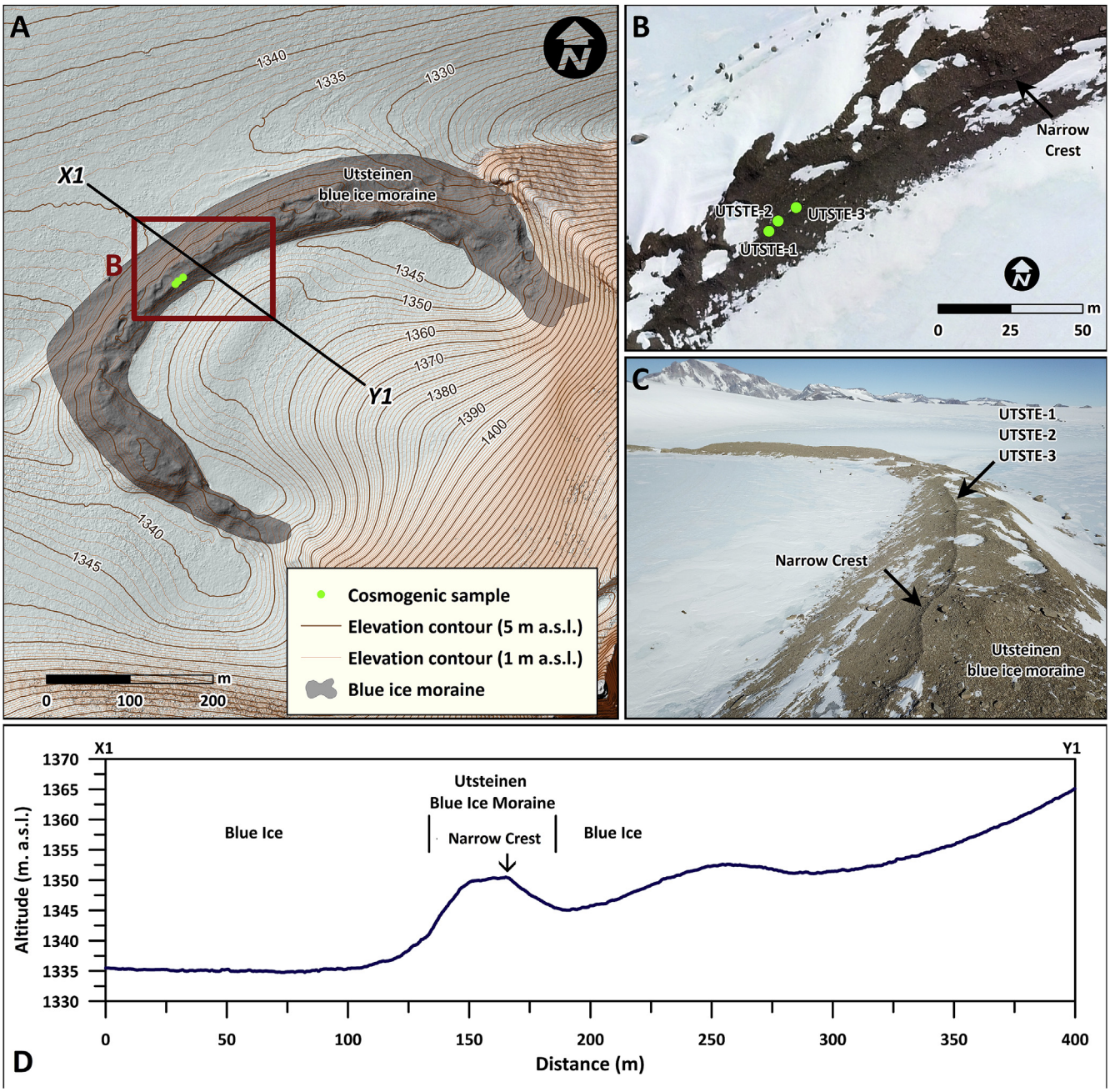

Fig. 2. The Utsteinen blue ice moraine. A: Orthoimage of the blue ice moraine and the Utsteinen nunatak. B: Close up view of the blue ice moraine, terminal moraine, and sample locations. C: Picture of the blue ice moraine and sampled terminal moraine, view towards southwest. D: Topographic profile X1-Y1.

Utsteinen (UTSTE) samples plot below the simple exposure line and the erosion island in the banana plot, indicating a complex exposure history (Fig. 8). In contrast to ^{10}Be and ^{Al}26 exposure ages, the in-situ cosmogenic ^{14}C analysis of these samples provide the following ages: for UTSTE-1, 4.6 ± 0.1 ka; for UTSTE-2, 5.7 ± 0.1 ka; and for UTSTE-3, 4.2 ± 0.1 ka. For this landform, we calculate a mean age of 4.4 ± 0.2 ka after identifying UTSTE-2 as an outlier because it resides beyond the two-sigma fence of the other two samples.

Ketelers blue ice moraine is built on the right lateral side of the Ketelers glacier and fed by sediments transported by five tributary cirques located to the east of the glacier. It is around 10 km long and reaches a maximum width of ca. 600 m. Here, we investigate the part of the moraine that is fed by the first two cirques (Fig. 4). This part is ~4.5 km long and 100–300 m wide. The moraine lies ~16 m above the ice (Fig. 4D) and shows dead-ice and permafrost features. It has a complex structure and contains several crest lines. It is composed of sediments from three different sources. The first group of sediments stem from the mainstream of the Ketelers glacier. The second group of sediments is the debris deposited directly on the ice as a product of gravitational processes, such as rock falls from the flanks of the nunatak in the upper part of the valley. In the Ketelers valley, sediment from these sources cannot be differentiated because there is not a distinct lithological differences of the bedrock. However, the debris, composed of sediments from both sources, is dominated by granitic lithologies, which is reflected in the light color of the deposit (Fig. 4B and C). The third group of sediments originates from the tributary cirques from the eastern side of the valley. The sediments from the first cirque in the southeastern part of the valley are mainly dark colored because of the metatonalitic bedrock associated with amphibole schists in the tributary cirque (Shiraishi et al., 1997). This contrast enabled us to differentiate between the deposits of the main

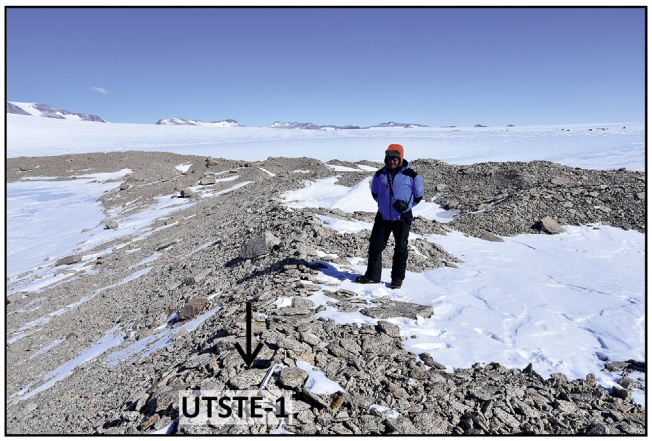

Fig. 3. Sampled slab UTSTE-1 on the terminal moraine, Utsteinen blue ice moraine, view toward the southwest.

ice stream, which includes both the first and second group of sediments, and the local terminal moraine of the cirque glacier (third group of sediments *sensu lato*). As the main ice flow dams the ones from the tributary, this local medial moraine deposited by the cirque glacier is displaced and deformed by the main ice stream, which is indicated by the formation of several ridges. From the high-resolution DEM, we evaluate ~700 m of total displacement for this local medial moraine (Fig. 4A and D). KETEL-1 yields a simple exposure history with an $^{26}Al/^{10}Be$ ratio of 7.01 ± 0.32 (Table 2, Figs. 5A and 8) and exposure ages of 108.9 ± 2.4 ka for ^{10}Be and 111.7 ± 3.5 ka for ^{26}Al. In contrast, results for KETEL-2 indicate a complex exposure history with a $^{26}Al/^{10}Be$ ratio of 5.91 ± 0.33. These two samples show a saturation for in-situ ^{14}C, which means a minimum exposure of 25 ka (calculated with a very conservative estimate of 5% uncertainty). For KETEL-3, we only calculate an ^{26}Al exposure age of 15.4 ± 1.1 ka (Table 4). Results from KETEL-4, 5, and 6 indicate complex exposure histories for cosmogenic ^{10}Be and ^{26}Al, with ratios of 5.77 ± 0.19, 5.55 ± 0.14 and 5.20 ± 0.13, respectively (Fig. 8). The in-situ ^{14}C analysis in KETEL-6 also indicates saturation. For KETEL-5, we evaluate an in-situ ^{14}C exposure age of 13.4 ± 03 ka (Table 4 and Fig. 5B).

The Dry blue ice moraine is the terminal moraine in the southwestern end of the Dry valley deposited by the Hargreaves glacier (Fig. 6). It is arcuate-shaped and ~1.5 km long and ~80 m wide on average, with a maximum width of ~140 m at its central part. The moraine lies 15 m above the snow/ice patch on the outer side and ~25 m above the blue ice on the inner side. However, it is ~30 m lower than the surface of the main blue ice in the west. DRY-5 exhibits a simple exposure history with an $^{26}Al/^{10}Be$ ratio of 6.99 ± 0.26 (Table 2 and Fig. 8). The calculated exposure ages of DRY-5 are 31.8 ± 1.1 ka for ^{10}Be and 32.1 ± 1.0 ka for ^{26}Al (Table 4). On the other hand, DRY-1, DRY-2, and DRY-3 indicate a complex history with $^{26}Al/^{10}Be$ ratios of 3.53 ± 0.20, 6.18 ± 0.21, and 6.33 ± 0.33. Only DRY-3 touches the simple exposure line within the two-sigma uncertainty (Fig. 8). For DRY-3, we calculate a ^{10}Be exposure age of 18.2 ± 0.6 ka and an ^{26}Al age of 16.5 ± 0.7 ka. The in-situ ^{14}C exposure age of DRY-3 is 22.2 ± 1.3 ka; for DRY-2 (^{10}Be: 31.3 ± 0.9; ^{26}Al: 27.8 ± 0.6 ka), the in-situ ^{14}C is saturated, indicating a minimum exposure age of ~25 ka (Table 4).

4.2. Sediment source of blue ice moraines

During the exploration of the blue ice moraines in the Sør Rondane Mountains, we identified two sediment sources in the field: the base of the glacier and nunataks in contact with ice. Nunataks can be considered a surficial source, from which supraglacial sediments can be laterally transported and/or directly deposited by surface processes such as rock falls. As well as to supraglacial input, nunataks feed the blue ice moraines through as well as the ice flow in the tributary cirques. The contribution of subsurface and surficial sources to the accretion of blue ice moraines is not always consistent and varies as per the presence of nearby nunataks, the ice flow regime, and bedrock geology (i.e., bear bedrock cliffs versus slopes made of loose debris). Unless there is a key lithology from a distinct source or sedimentological features such as glacial polish, the source of the clasts in a blue ice moraine is hard to distinguish. On the one hand, the differentiation of the sediments from the main ice stream and tributary ice is evident in the Ketelers blue ice moraine because of the color difference in the bedrock lithology and the displacement caused by the main ice stream (Fig. 4). On the other hand, as the Utsteinen nunatak is composed of one lithology, whether the sediments originate from the base of the local ice tongue or not remains unclear (Fig. 2).

5. Discussion

5.1. Chronology of the blue ice moraines

In this study, we reconstructed the chronologies of three blue ice moraines using surface exposure dating with multiple cosmogenic nuclides (Table 4). Cosmogenic ^{10}Be and ^{26}Al ratios of DRY-1, DRY-2 and DRY-3 show complex exposure histories (Fig. 8). Based only on the simple exposure indicated by the cosmogenic ^{10}Be and ^{26}Al analysis from DRY-5 (Fig. 8), one could conclude that the Dry blue ice moraine was deposited at around 32 ka. However, in-situ ^{14}C analysis on DRY-3 indicate an exposure age of 22.0 ± 1.3 ka. The saturation of in-situ ^{14}C in DRY-2 also indicates a simple exposure for at least 25 ka, which is in line with the data from ^{10}Be and ^{26}Al data from DRY-5, as well as with the in-situ ^{14}C data from DRY-2. We explain the discrepancy between the simple exposure for around 32 ka shown by cosmogenic ^{10}Be and ^{26}Al measured in DRY-5 (Fig. 8) and by in-situ ^{14}C measured in DRY-3 as follows. Although DRY-5 penetrates into the complex exposure zone within the uncertainties, this cobble could have been sublimated a few thousand years earlier on the ice, and then deposited on DRY-4. In such a case, we expect a saturated in-situ ^{14}C signal from DRY-5. Based on these lines of evidence, we consider 22.0 ± 1.3 ka as the maximum age of the landform and conclude that the Dry blue ice moraine was deposited during the LGM (22.3 ± 3.6 ka in the Southern Hemisphere; Shakun and Carlson, 2010).

In the Ketelers blue ice moraine, KETEL-2, KETEL-4, KETEL-5, and KETEL-6 yield complex exposure histories in contrast to KETEL-1, which shows a simple exposure history (Fig. 8). Based on this simple exposure history, one could suppose that the Dry blue ice moraine was deposited at ~110 ka. In addition, KETEL-1, KETEL-2, and KETEL-6 show saturated in-situ ^{14}C concentrations. We regard this saturation signal as an indication for simple exposure conditions during at least the last 25 ka. However, KETEL-5 gives an in-situ ^{14}C exposure age of 13.4 ± 0.3 ka. In this case, one could argue that the part of the blue ice moraine deposited by the main ice stream dates back to ~110 ka, as KETEL-1, KETEL-2, and KETEL-3 were collected from the outermost crest of this part. On the other hand, the part deposited by the tributary ice can be attributed to ~13 ka. We think that this scenario is unlikely based on the displacement of the sediments from the tributary cirque by the main ice stream (Fig. 4). Therefore, we explain the simple ^{10}Be and ^{26}Al exposure history of KETEL-1 as a result of the deposition of a granitic boulder, which was exposed during or at the end of the Last Interglacial (130–115 ka; cf. DeConto and Pollard, 2016) in the right lateral side of the Ketelers glacier. Alternatively, KETEL-1 could stem from the granite bedrock (located around 2 km up valley) that collapsed on the ice during or at the end of the Last Interglacial and was then transported as a supraglacial sediment to today's position. In brief, we conclude that the Ketelers blue ice moraine was built during the last deglaciation and not later than the Lateglacial (cf. Shakun and Carlson, 2010) based on the in-situ ^{14}C exposure age of KETEL-5.

In the Utsteinen blue ice moraine, we date the most prominent narrow crest to the mid-Holocene (4.4 ± 0.2 ka). The main body of the

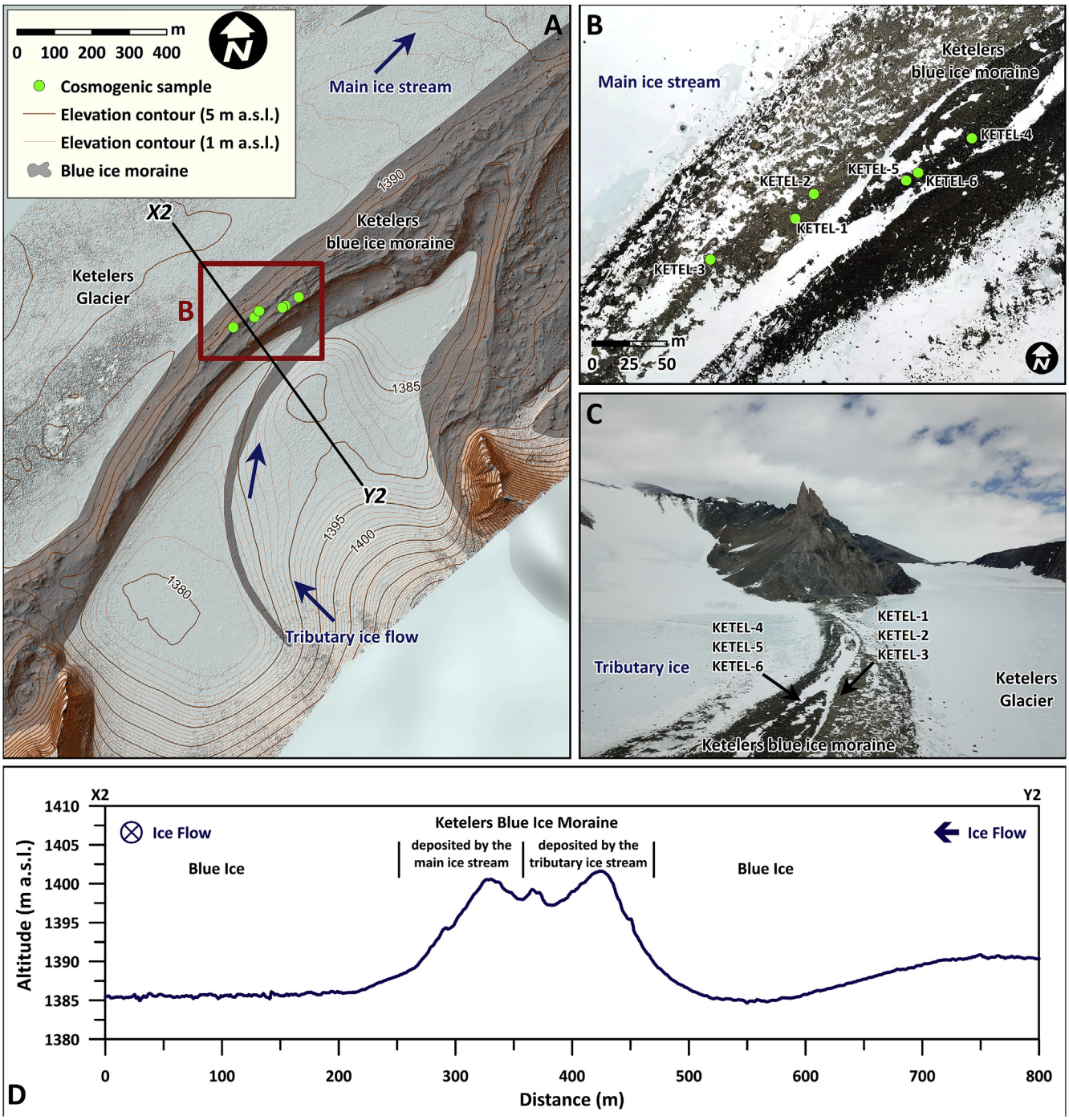

Fig. 4. The Ketelers blue ice moraine. A: Orthoimage of the blue ice moraine. B: Close up view of the blue ice moraine and sample locations. C: Picture of the blue ice moraine and sampled ridges, view toward the southwest. D: Topographic profile X2-Y2.

moraine should then be older than the mid-Holocene. The cosmogenic ^{10}Be and ^{26}Al concentrations in all UTSTE samples indicate complex exposure histories, thus, inherited concentrations. We argue that this inheritance is a result of the accumulation of ^{10}Be and ^{26}Al either at the surface of Utsteinen nunatak, which might have repeatedly been covered and exposed in the past, or at depth in the pegmatitic bedrock. As the ^{26}Al/^{10}Be ratio might be as high as 8.4 in the case of a pure accumulation at greater depth (cf. Akçar et al., 2017), we conclude based on the ^{26}Al/^{10}Be ratios that these slabs were at or close to the bedrock surface, which were exposed for tens of thousands of years (e.g., ~100 ka), and then buried or covered by ice until the inheritance signal for in-situ ^{14}C was completely deleted (~30 ka). Based on these results, we conclude that the accumulation of blue ice moraines explored and dated in this study commenced during and after the LGM.

Existing cosmogenic nuclide chronologies of the Antarctic blue ice moraines were mainly built on the analysis of cosmogenic ^{10}Be, supported by a limited number of ^{26}Al measurements. In addition, cosmogenic ^{21}Ne and ^{36}Cl were also measured at a few locations (e.g., Hein et al., 2016). The blue ice moraines were generally sampled along the accumulation direction of the moraine, from the inner/younger ridge towards the outer/older ridge (e.g., Altmaier et al., 2010). The ^{10}Be exposure ages span a time spectrum from a few hundred to a few hundred thousand years. Except for some sediments exposed for a few hundred thousand years, old exposure ages generally cluster around 100 ka. There

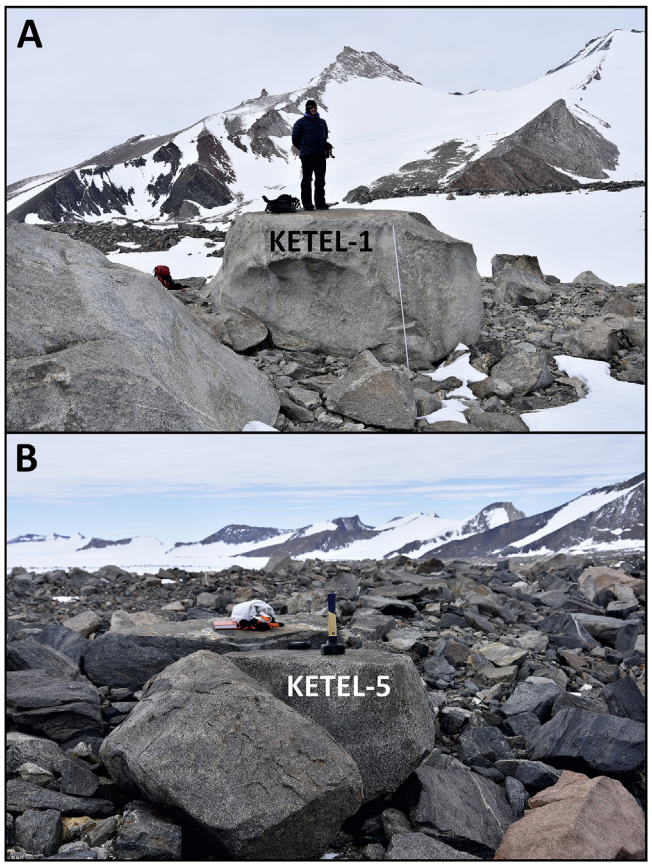

Fig. 5. A: Sampled Boulder KETEL-1 on the Ketelers blue ice moraine, view toward the northeast. B: Boulder KETEL-5 (1.1 m long, 1.1 m wide and 0.8 m high) on the Ketelers blue ice moraine, view toward the northeast.

is a trend in the distribution of the exposure ages; generally, they are coherent with the built-up of the blue ice moraines, i.e., exposure ages increase from the inner toward the outer ridges. $^{26}Al/^{10}Be$ ratios, which are above or close to the surface ratio line, or hit it within the uncertainty ranges, are considered as an indication for a simple exposure or for complex exposure histories shorter than 100 ka (e.g., Kaplan et al., 2017).

In our study, we follow a slightly different sampling strategy. We collect three to five samples per landform, e.g., the outermost ridge of the main ice stream of the Ketelers blue ice moraine (Fig. 4). In this way, we do not reconstruct the chronology of the blue ice moraine evolution, but we date either the beginning of their build-up (e.g., the Ketelers BIM) or the last pulse of accumulation (e.g., the Utsteinen blue ice moraine) (Figs. 2 and 4). While analyzing cosmogenic ^{10}Be and ^{26}Al, we encounter a similar range of exposure ages as compared to those reported in previously published studies (Altmaier et al., 2010; Fogwill et al., 2012; Suganuma et al., 2014; Hein et al., 2016; Kaplan et al., 2017). Our exposure ages range between ~15 ka and 690 ka (Table 4). Most of the $^{26}Al/^{10}Be$ ratios indicate complex exposure histories, whereas only a few indicate simple exposure histories, which might suggest limited short-term complexities in the exposure. However, the analysis of in-situ cosmogenic ^{14}C biases the ^{10}Be and ^{26}Al results, especially in the Utsteinen und Ketelers blue ice moraines (Fig. 8). This bias shows that the inheritance in old landscapes can obscure the real exposure histories, especially those shorter than a few ten thousand years. In addition, cosmogenic ^{10}Be and ^{26}Al might not be precise enough to disentangle this masked exposure histories, although they might signify a simple exposure history. Such camouflage can alter the chronology and, thus, its implications. For example, a vertical ice surface lowering of 6 m at the Utsteinen Nunatak will yield different sublimation rates depending on the reconstructed chronology of the terminal moraines on the blue ice moraine: ~0.05 mm/yr in case of sublimation since the Last Interglacial or ~1.2 mm/yr since the mid-Holocene. Keeping all this in mind, we strongly suggest the consideration of the in-situ ^{14}C analysis in addition to, and after the measurement of cosmogenic ^{10}Be and ^{26}Al to rule out any potential camouflage effects of the real exposure history by the inheritance. We also believe that the efficacy of the in-situ ^{14}C analysis in disentangling complex exposure histories is not limited to Antarctica: it also applies to the glacial landscapes where glacial erosion may not be sufficient enough to remove existing cosmogenic nuclides, i.e., zeroing the inheritance, such as in Scandinavia (cf. Jansen et al., 2019).

5.2. Sediment source and its effects on cosmogenic nuclide accumulation

The source of the material supplying the blue ice moraine has a great influence on the cosmogenic nuclide inventory of the material. For instance, surficial sediment input such as slope debris captured gradually by the ice will yield high cosmogenic ^{10}Be and ^{26}Al concentrations and $^{26}Al/^{10}Be$ ratios significantly lower than the surface ratio, thus indicating complex exposure histories, i.e. multiple exposure-burial cycles (e.g., Bierman et al., 1999; Fabel et al., 2002; Kaplan et al., 2017). In contrast, a cosmogenic nuclide inheritance in sediments from the ice base or deeper levels of the ice, which are conveyed to the surface so as to compensate the sublimation, will be zero or at a minimum, as, for instance, indicated by Fogwill et al. (2012). These sediments will generate simple or close to simple ^{10}Be and ^{26}Al exposure histories within the given uncertainty level (e.g., Kaplan et al., 2017). The in-situ ^{14}C signal, however, will depend on the exposure time, and the pre-LGM or early LGM exposure will show a saturation. For the LGM and later exposures, the in-situ ^{14}C concentrations will be consistent with those of ^{10}Be and ^{26}Al.

As a result of ice volume fluctuations during the glacial cycles, ice thickness oscillations can cause cycles of exposure and burial (cf. Fogwill et al., 2012; Kassab et al., 2019). These cycles will cause an inheritance of cosmogenic nuclides in the englacial or subglacial sediments. Depending on the duration of the exposure and burial cycles, the cosmogenic ^{10}Be and ^{26}Al data will indicate complex or close to simple exposure histories (e.g., Bierman et al., 1999; Fabel, 2002; Akçar et al., 2017). For burial cycles longer than ~100 ka, a complex exposure history will be indicated by the ^{10}Be and ^{26}Al isotopes. Because of the half-lives of the cosmogenic ^{10}Be and ^{26}Al (Norris et al., 1983; Nishiizumi, 2004; Chmeleff et al., 2010; Korschinek et al., 2010), shorter burial cycles will lead to an apparent close to simple exposure history (e.g., Kaplan et al., 2017). Thus, ^{10}Be and ^{26}Al are not competent enough to detect burial and exposure cycles within a time range $<$100 ka (cf. Granger and Muzikar, 2001). The analysis of in-situ ^{14}C has high potential to play a key role in disentangling the complex exposure histories within a time range shorter than approximately 100 ka. However, in-situ ^{14}C values will only help to unravel LGM and Post-LGM timescales, as mentioned above. Otherwise, in-situ ^{14}C values will yield saturation. The key requirement for a non-saturated in-situ ^{14}C signal, with which an exposure age could be calculated, is that the last period of burial prior to the final exposure has to be $>$ 30 ka, so that the all of the in-situ ^{14}C accumulated in the clast during the last pre-burial exposure decays, i.e., the clast reaches the surface with zero in-situ ^{14}C concentration. In this way, in-situ ^{14}C values will decipher the most realistic exposure history independent of the exposure history indicated by the ^{10}Be and ^{26}Al ratios.

5.3. Sediment source and its potential influences on inheritance

The base of the glacier is considered as the main source of debris that forms the blue ice moraines (Altmaier et al., 2010; Fogwill et al., 2012; Kaplan et al., 2017 among others). Altmaier et al. (2010) proposed that the sediments forming the Schüssel blue ice moraine originated from the base of the glacier, entrained at the wet-based and ground-based ice boundary and then conveyed to the surface as a result of the ice flow balanced by sublimation. Fogwill et al. (2012) argued that the blue ice

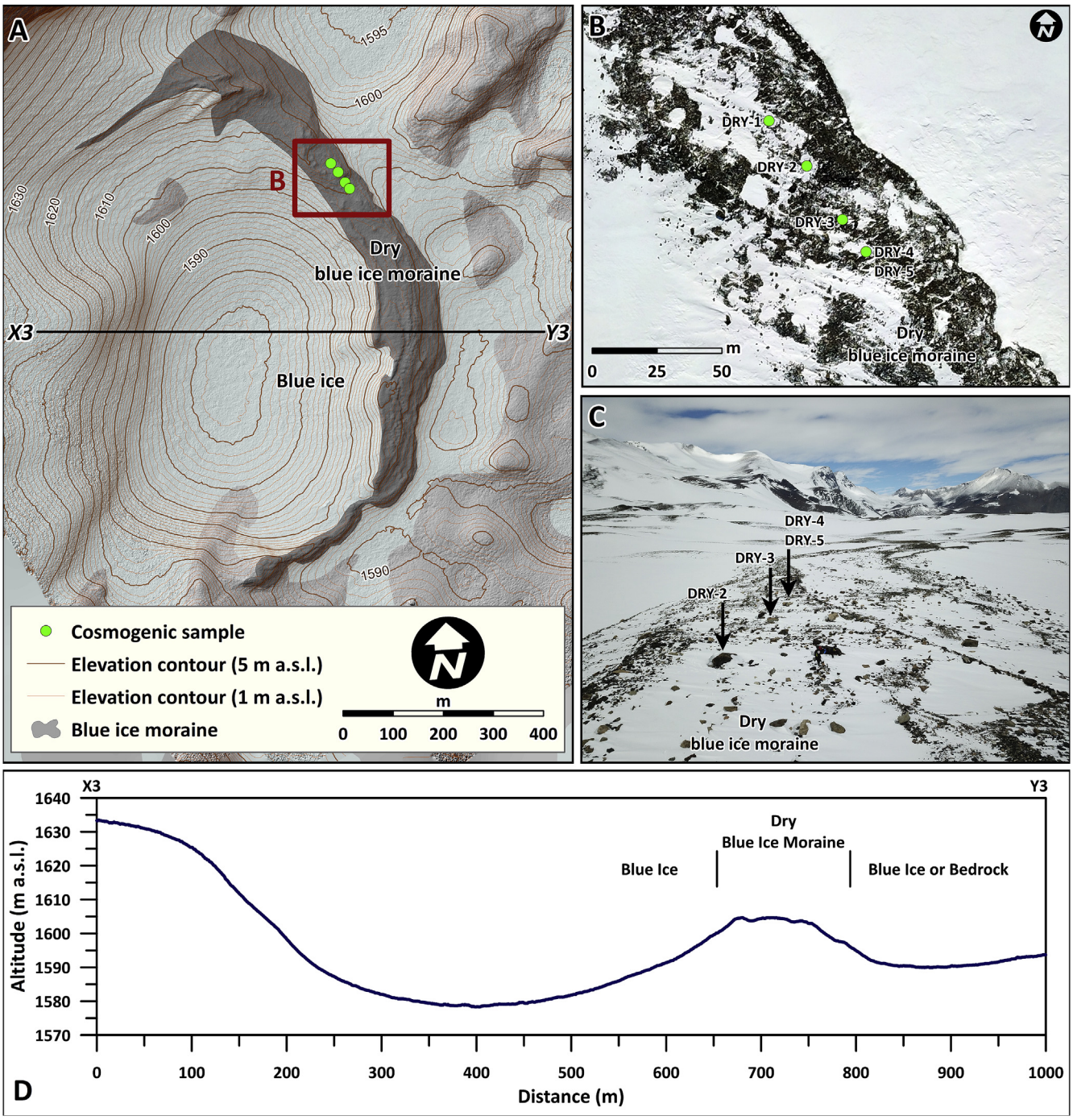

Fig. 6. The Dry blue ice moraine. A: Orthoimage of the blue ice moraine. Contour interval is 20 m. B: Close up view of the blue ice moraine and sample locations. C: Picture of the blue ice moraine and sampled boulders, view toward the southeast. D: Topographic profile X3-Y3.

moraines in the Patriot Hills are equilibrium landforms with two requirements. Firstly, the sediments building the blue ice moraines were derived from the base of the glacier and not laterally displaced, although they seem to be derived from nunataks at first sight. Secondly, a dynamic ice flow regime is required to move basal sediments to the surface where they are stored. Based on the field evidence and cosmogenic ^{10}Be concentrations in two clasts, which were randomly collected from the ice surface, Fogwill et al. (2012) ruled out any sediment contribution from the surrounding nunataks. Kaplan et al. (2017) argued that significant inheritance should exist in the case of sediment input from the surrounding bedrock headwalls for the Mount Achernar blue ice moraine. Based on their multiple cosmogenic nuclide analysis and field observations, they assumed that the upward-flowing ice acquired the sediments from the base of the ice and transported them to the surface. The provenance analysis of Bader et al. (2017) and the stable isotope analysis in ice cores from the blue ice moraine (Graly et al., 2018) supported the interpretations of Kaplan et al. (2017).

DRY-1 in our sample set might be an example for having a surficial sediment source, because it yielded high cosmogenic ^{10}Be and ^{26}Al concentrations and a low ^{26}Al/^{10}Be ratio (Fig. 8). The analysis of the in-situ ^{14}C in the surficial sediments will point toward a saturation. We cannot exclude the possibility that any deep-seated mass movement could expose pristine sediments to cosmic rays without any inheritance. In that case, however, the cosmic ray clock will record the timing of

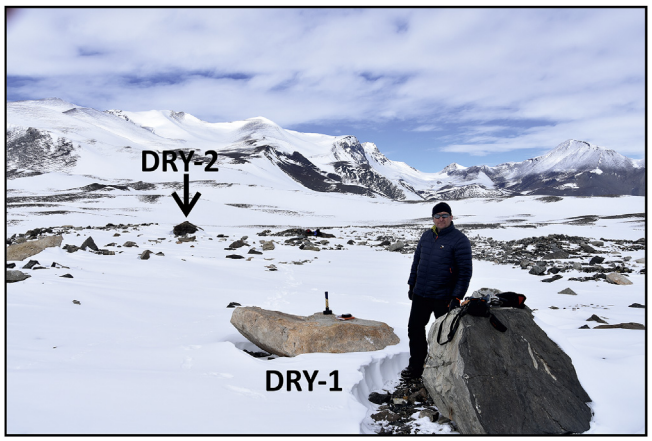

Fig. 7. Surface exposure dating samples DRY-1 and DRY-2 on the Dry blue ice moraine, view toward the southeast.

failure and not the formation of the blue ice moraine. In addition, to gauge an inheritance within the measurement uncertainties, which will have been accumulated because of the muonic production of cosmogenic nuclides at depth in an old landscape like Antarctica, we expect the failure surface should be located at a depth of at least ~100 m. When we consider that Akçar et al. (2014) identified an inheritance in a 300-year old rock avalanche deposit from 1717 AD, we believe that the probability of having surficial sediments without an inheritance is unlikely.

Considering the high costs, time, and personal requirements of the multiple cosmogenic nuclide analysis, we finally argue that the identification of a basal clast in a blue ice moraine is crucial. Far travelled erratic sediments, unless they are reworked, seem to be the best candidates for sampling (cf. Bader et al., 2017). Here, the definition of "erratic" strongly depends on the bedrock lithology of the nunatak that hosts the blue ice moraine. For instance, a piece of a magmatic rock on a volcanic terrain is undoubtedly an erratic. However, the identification of an erratic might not be always obvious. Considering the fact that the target erratic clast should bear quartz for the multiple cosmogenic nuclide analysis, the detection of an erratic clast in a metamorphic terrain intruded by plutonic rocks, such as the Sør Rondane Mountains (Shiraishi

Table 2
Cosmogenic ^{10}Be and ^{26}Al data of the samples from the Sør Rondane Mountains.

Sample Name	Quartz dissolved (g)	^{9}Be Spike (mg)	^{10}Be (x10^{6} at/g)	Total Al (mg)	^{26}Al (x10^{6} at/g)	^{26}Al/^{10}Be
UTSTE-1	36.1617	0.1751	1.85 ± 0.04	0.53	11.76 ± 0.18	6.36 ± 0.16
UTSTE-2	36.7781	0.1751	1.93 ± 0.04	0.60	12.06 ± 0.19	6.26 ± 0.16
UTSTE-3	37.2306	0.1753	1.30 ± 0.03	0.59	8.01 ± 0.14	6.15 ± 0.17
DRY-1	25.0836	0.1750	12.29 ± 0.53	38.97	43.44 ± 1.53	3.53 ± 0.20
DRY-2	25.0311	0.1759	0.68 ± 0.02	0.52	4.18 ± 0.09	6.18 ± 0.21
DRY-3	25.3153	0.1743	0.40 ± 0.01	1.84	2.53 ± 0.11	6.33 ± 0.33
DRY-4	25.2445	0.1746	3.26 ± 0.11	43.06	n.a.	n.a.
DRY-5	25.2526	0.1741	0.68 ± 0.02	0.91	4.79 ± 0.14	7.01 ± 0.32
KETEL-1	20.1098	0.1752	1.99 ± 0.04	10.35	13.88 ± 0.42	6.99 ± 0.26
KETEL-2	20.1484	0.1741	1.89 ± 0.06	40.75	11.16 ± 0.50	5.91 ± 0.33
KETEL-3	29.6360	0.1753	n.a.	34.26	1.99 ± 0.14	n.a.
KETEL-4	29.7589	0.1751	1.00 ± 0.03	2.71	5.76 ± 0.11	5.77 ± 0.19
KETEL-5	40.1405	0.1742	5.51 ± 0.11	1.26	30.58 ± 0.43	5.55 ± 0.14
KETEL-6	40.0059	0.1754	7.38 ± 0.15	1.33	38.32 ± 0.54	5.20 ± 0.13

Accelerator mass spectrometer (AMS) measurement errors are at 1s level, including the statistical (counting) error and the error due to normalization of standards and blanks. The error weighted average ^{10}Be/^{9}Be full-process blank ratio is (2.37 ± 0.62) x 10^{-15}. ^{26}Al/^{10}Be ratios were calculated with the CRONUS-Earth exposure age calculator and were referenced to 07KNSTD (Balco et al., 2008 and update from v. 2.2 to v. 2.3 published by Balco in June 2016; http://hess.ess.washington.edu/math/al_be_v23/al_be_multiple_v23.html).

Table 3
In-situ ^{14}C data of the samples from the Sør Rondane Mountains.

Sample Name	AMS ID	Sample mass (g_{qtz})	CO_2 yield (μg)[a]	Fraction modern F^{14}C[b]	δ^{13}C (‰)	^{14}C/$^{12}C_{abs}$ (10^{-12})	Subtracted blank (10^{4} atoms ± 1SD)	^{14}C conc. (10^{4} at/g)[c]
UTSTE-1	96051.1.1	3.7938	19.89	0.646 ± 0.008	0.7	0.781 ± 0.010	2.660 ± 1.030	19.818 ± 0.379
UTSTE-2	96052.1.1	3.7688	20.56	0.723 ± 0.009	−1.0	0.870 ± 0.011	2.660 ± 1.030	23.096 ± 0.399
UTSTE-3	97376.1.1	4.0191	20.77	0.640 ± 0.007	−19.5	0.742 ± 0.008	2.660 ± 1.030	18.568 ± 0.333
DRY-2	104476.1.1	3.9594	25.99	1.575 ± 0.013	−5.9	1.877 ± 0.015	5.726 ± 0.580	60.340 ± 0.514
DRY-3	96050.1.1	3.8248	47.39	0.729 ± 0.007	−4.1	0.873 ± 0.009	2.660 ± 1.030	53.519 ± 0.611
KETEL-1	104472.1.1	4.0917	16.75	2.790 ± 0.020	−2.5	3.349 ± 0.024	5.726 ± 0.580	67.321 ± 0.507
KETEL-2	104473.1.1	4.1851	17.02	2.888 ± 0.020	−3.9	3.456 ± 0.024	5.726 ± 0.580	69.099 ± 0.515
KETEL-5	104474.1.1	4.0111	20.72	1.319 ± 0.011	−4.5	1.577 ± 0.014	5.726 ± 0.580	39.411 ± 0.384
KETEL-6	104475.1.1	4.1460	18.61	2.021 ± 0.015	−3.0	2.423 ± 0.018	5.726 ± 0.580	53.162 ± 0.433

[a] CO_2 yield includes ca.15 μg of ^{14}C-free CO_2, which was added as a carrier gas prior to extraction (Lupker et al., 2019).
[b] Normalized to δ^{13}C of −25‰VPDB and 1950.
[c] All uncertainties are ± 1σ and include uncertainties related to AMS measurement and the subtracted blank.

Table 4
Surface exposure ages of the samples from the Sør Rondane Mountains.

Sample Name	^{10}Be Exposure Age (ka)		^{26}Al Exposure Age (ka)		In-situ ^{14}C Exposure Age (ka)		Landform Age (ka)
UTSTE-1	107.2 ± 2.2	(8.5)	99.4 ± 1.6	(9.9)	4.6 ± 0.1	(0.3)	4.4 ± 0.2
UTSTE-2	112.9 ± 2.3	(9.0)	103.1 ± 1.7	(10.3)	5.7 ± 0.1	(0.4)	
UTSTE-3	75.4 ± 1.7	(6.0)	67.1 ± 1.2	(6.6)	4.2 ± 0.1	(0.3)	
KETEL-1	108.9 ± 2.4	(8.8)	111.7 ± 3.5	(11.6)	*saturated*		13.4 ± 0.3
KETEL-2	103.9 ± 3.6	(8.8)	89.1 ± 4.2	(9.7)	*saturated*		
KETEL-3	n.a.		15.4 ± 1.1	(1.8)			
KETEL-4	54.5 ± 1.5	(4.4)	45.3 ± 0.9	(4.4)			
KETEL-5	319.7 ± 6.9	(26.9)	265.9 ± 4.3	(28.9)	13.4 ± 0.3	(1.7)	
KETEL-6	443.5 ± 9.9	(38.5)	348.2 ± 5.8	(39.5)	*saturated*		
DRY-1	659.5 ± 33.9	(68)	332.0 ± 13.9	(39)			22.0 ± 1.3
DRY-2	31.3 ± 0.9	(2.5)	27.8 ± 0.6	(2.7)	*saturated*		
DRY-3	18.2 ± 0.6	(1.5)	16.5 ± 0.7	(1.7)	22.0 ± 1.3	(5.6)	
DRY-4	155.7 ± 5.4	(13)	n.a.				
DRY-5	31.8 ± 1.1	(2.6)	32.1 ± 1.0	(3.2)			

Cosmogenic ^{10}Be, ^{26}Al and in-situ ^{14}C exposure ages were calculated with the CRONUS-Earth exposure age calculator (http://hess.ess.washington.edu/math/v3/v3_age_in.html; Balco et al., 2008). Local production rates of cosmogenic nuclides were scaled using time dependent Lal (1991)/Stone (2000) scaling scheme. Exposure ages are corrected for dip of rock surface, shielding of surrounding topography, and sample thickness, but not corrected for erosion and snow cover, as explained in the text.The combined uncertainties of exposure ages due to AMS measurements and due to uncertainties in production rate parameters are given in parentheses.

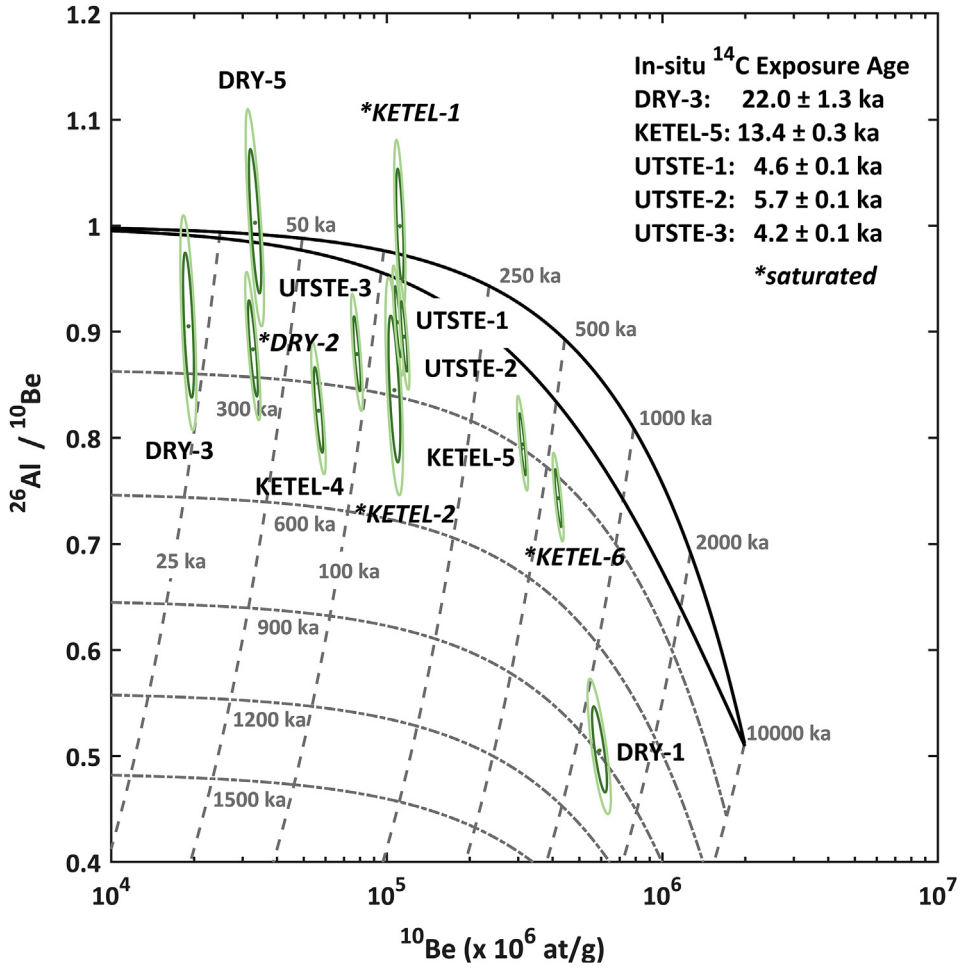

Fig. 8. ^{26}Al–^{10}Be banana plot of the blue ice moraine samples analyzed in this study. In-situ ^{14}C exposure ages are also provided. This plot was computed with the iceTEA tool (http://ice-tea.org), MATLAB® code provided by Jones et al. (2019), with the time dependent Lal (1991)/Stone (2000) scaling model.

et al., 1997), could be critical. Thus, the lithology might help to find the most suitable clast for cosmogenic nuclide analysis.

Finally, we provide data which show that the sediment source for the build-up of blue ice moraines could play a substantial role in the cosmogenic nuclide inheritance in the analyzed clasts. Based on our in-situ ^{14}C results, we also show that blue ice moraines can be younger than indicated by simple or close to simple exposure histories based on cosmogenic ^{10}Be and ^{26}Al analysis. To clear up the complexities in the building processes of the blue ice moraines and their short- and long-term evolution, there is a substantial need for more studies, which will indeed improve our understanding of the changes in ice sheet dynamics as well as the accumulation of micrometeorites (e.g., Genge et al., 2018) and the

evolution of microbial activity (e.g., Tytgat et al., 2016) in Antarctica.

6. Conclusions

We applied geomorphological and multiple cosmogenic nuclide analyses to the blue ice moraines in the Sør Rondane Mountains, Queen Maud Land in Antarctica, whose chronostratigraphy remains inadequately reconstructed, to study the capability of in-situ cosmogenic ^{10}Be and ^{26}Al and investigate the relationship between the sediment source and accumulation of cosmogenic nuclides. In the field, we observed the following sediment sources for the studied blue ice moraines, namely the base of the ice and the nunataks. We found that the identification of the origin of the sediments, either from the ice base or surface is difficult if any sedimentological or lithological criterion is not evident. We processed a total of 14 rock surface samples from the Utsteinen, Ketelers, and Dry Valley blue ice moraines for surface exposure dating. We measured cosmogenic ^{10}Be, ^{26}Al, and in-situ ^{14}C in these samples. The cosmogenic ^{10}Be and ^{26}Al results showed complex, close to simple, and simple exposure histories. The analysis of in-situ ^{14}C indicated a younger chronology in contrast to the ^{10}Be and ^{26}Al chronology, which was inferred by the close to simple and simple exposure histories.

Our ^{10}Be and ^{26}Al chronology is in line with the existing blue ice moraine chronologies. However, our younger in-situ ^{14}C chronology with respect to the cosmogenic ^{10}Be and ^{26}Al chronology, which indicated close to simple and simple exposure histories, suggest that the cosmogenic ^{10}Be and ^{26}Al chronologies may not be competent enough to resolve the blue ice moraines' timing of their accumulation and evolution, and thus, cosmogenic ^{10}Be and ^{26}Al without in-situ ^{14}C may potentially lead to misinterpretations. Based on these, we concluded that the application of in-situ ^{14}C analysis in the investigation of the blue ice moraines is essential and certainly be key tool in discovering their evolution during the last 100 ka, especially in the last 30 ka. Nonetheless, blue ice moraines bear the records of ice sheet fluctuations, trap wind transported micrometeorites, and hosts evidences life's evolution in Antarctica. Therefore, they merit special attention in discovering the Antarctic glaciation, and related global changes.

Declaration of competing interest

The authors declare that they have no known competing financial interests or personal relationships that could have appeared to influence the work reported in this paper.

Acknowledgements

We would like to thank Polar Research Center team at the Istanbul Technical University for organizing our participation in the BELARE 2017–2018 Expedition within the bilateral scientific collaboration program of the second Turkish Antarctic Expedition, TAE-II 2017–2018. We are grateful to thank Alain Hubert, Nighat Amin, and Michel de Wouters at the International Polar Foundation for their support both in the logistics and field. We would also like to thank the Princess Elisabeth Antarctica Research Station Team for their support during our field campaign. We are also grateful to the Laboratory of Ion Beam Physics accelerator mass spectrometry facility operated by the Swiss Federal Institute of Technology, Zurich, Switzerland. This study was carried out under the auspices of the Turkish Republic Presidency, supported by the Ministry of Science, Industry and Technology, and coordinated by Istanbul Technical University Polar Research Center (ITU PolRec). It was financed by the ITU PolRec, Swiss National Science Foundation [grant number 200021–172475], Swiss Polar Institute, and University of Bern.

Appendix A. Supplementary data

Supplementary data to this article can be found online at https://doi.org/10.1016/j.qsa.2020.100012.

References

Akçar, N., Deline, P., Ivy-Ochs, S., Alfimov, V., Hajdas, I., Kubik, P.W., Christl, M., Schluchter, C., 2012. The AD 1717 rock avalanche deposits in the upper Ferret Valley (Italy): a dating approach with cosmogenic Be-10. J. Quat. Sci. 27, 383–392.

Akçar, N., Ivy-Ochs, S., Alfimov, V., Schlunegger, F., Claude, A., Reber, R., Christl, M., Vockenhuber, C., Dehnert, A., Rahn, M., Schluchter, C., 2017. Isochron-burial dating of glaciofluvial deposits: first results from the Swiss Alps. Earth Surf. Process. Landforms 42, 2414–2425.

Akçar, N., Ivy-Ochs, S., Deline, P., Alfimov, V., Kubik, P.W., Christl, M., Schluchter, C., 2014. Minor inheritance inhibits the calibration of the Be-10 production rate from the AD 1717 Val Ferret rock avalanche, European Alps. J. Quat. Sci. 29, 318–328.

Akçar, N., Ivy-Ochs, S., Kubik, P.W., Schlüchter, C., 2011. Post-depositional impacts on 'Findlinge' (erratic boulders) and their implications for surface-exposure dating. Swiss J. Geosci. 104, 445–453.

Altmaier, M., Herpers, U., Delisle, G., Merchel, S., Ott, U., 2010. Glaciation history of Queen Maud Land (Antarctica) reconstructed from in-situ produced cosmogenic Be-10, Al-26 and Ne-21. Pol. Sci. 4, 42–61.

Bader, N.A., Licht, K.J., Kaplan, M.R., Kassab, C., Winckler, G., 2017. East Antarctic ice sheet stability recorded in a high-elevation ice-cored moraine. Quat. Sci. Rev. 159, 88–102.

Balco, G., Stone, J.O., Lifton, N.A., Dunai, T.J., 2008. A complete and easily accessible means of calculating surface exposure ages or erosion rates from Be-10 and Al-26 measurements. Quat. Geochronol. 3, 174–195.

Bierman, P.R., Marsella, K.A., Patterson, C., Davis, P.T., Caffee, M., 1999. Mid-Pleistocene cosmogenic minimum-age limits for pre-Wisconsinan glacial surfaces in southwestern Minnesota and southern Baffin island: a multiple nuclide approach. Geomorphology 27, 25–39.

Bintanja, R., 1999. On the glaciological, meteorological, and climatological significance of Antarctic blue ice areas. Rev. Geophys. 37, 337–359.

Chmeleff, J., von Blanckenburg, F., Kossert, K., Jakob, D., 2010. Determination of the Be-10 half-life by multicollector ICP-MS and liquid scintillation counting. Nucl. Instrum. Methods Phys. Res. Sect. B Beam Interact. Mater. Atoms 268, 192–199.

Christl, M., Vockenhuber, C., Kubik, P.W., Wacker, L., Lachner, J., Alfimov, V., Synal, H.A., 2013. The ETH Zurich AMS facilities: performance parameters and reference materials. Nucl. Instrum. Methods Phys. Res. Sect. B Beam Interact. Mater. Atoms 294, 29–38.

Corti, G., Zeoli, A., Belmaggio, P., Folco, L., 2008. Physical modeling of the influence of bedrock topography and ablation on ice flow and meteorite concentration in Antarctica. J. Geophys. Res. Earth. Surface. 113, F01018.

DeConto, R.M., Pollard, D., 2016. Contribution of Antarctica to past and future sea-level rise. Nature 531, 591.

Dunai, T.J., 2010. Cosmogenic Nuclides Principles, Concepts and Applications in the Earth Surface Sciences. Cambridge University Press, Cambridge.

Dunne, J., Elmore, D., Muzikar, P., 1999. Scaling factors for the rates of production of cosmogenic nuclides for geometric shielding and attenuation at depth on sloped surfaces. Geomorphology 27, 3–11.

Fabel, D., Stroeven, A.P., Harbor, J., Kleman, J., Elmore, D., Fink, D., 2002. Landscape preservation under Fennoscandian ice sheets determined from in situ produced Be-10 and Al-26. Earth Planet Sci. Lett. 201, 397–406.

Faure, G., Grootes, P., Buchanan, D., Hagen, E.H., 1992. Oxygen isotope study of the ice fields surrounding the Reckling Moraine on the East Antarctic ice sheet. In: Elliot, D.H. (Ed.), Contributions to Antarctic Research. Antarctic Research Series, III, 57. American Geophysical Research, Washington, DC, pp. 15–26.

Fireman, E.L., Rancitelli, L.A., Kirsten, T., 1979. Terrestrial ages of 4 allan Hills meteorites - consequences for antarctic ice. Science 203, 453–455.

Fogwill, C.J., Hein, A.S., Bentley, M.J., Sugden, D.E., 2012. Do blue-ice moraines in the Heritage Range show the West Antarctic ice sheet survived the last interglacial? Palaeogeogr. Palaeoclimatol. Palaeoecol. 335, 61–70.

Fretwell, P., Pritchard, H.D., Vaughan, D.G., Bamber, J.L., Barrand, N.E., Bell, R., Bianchi, C., Bingham, R.G., Blankenship, D.D., Casassa, G., Catania, G., Callens, D., Conway, H., Cook, A.J., Corr, H.F.J., Damaske, D., Damm, V., Ferraccioli, F., Forsberg, R., Fujita, S., Gim, Y., Gogineni, P., Griggs, J.A., Hindmarsh, R.C.A., Holmlund, P., Holt, J.W., Jacobel, R.W., Jenkins, A., Jokat, W., Jordan, T., King, E.C., Kohler, J., Krabill, W., Riger-Kusk, M., Langley, K.A., Leitchenkov, G., Leuschen, C., Luyendyk, B.P., Matsuoka, K., Mouginot, J., Nitsche, F.O., Nogi, Y., Nost, O.A., Popov, S.V., Rignot, E., Rippin, D.M., Rivera, A., Roberts, J., Ross, N., Siegert, M.J., Smith, A.M., Steinhage, D., Studinger, M., Sun, B., Tinto, B.K., Welch, B.C., Wilson, D., Young, D.A., Xiangbin, C., Zirizzotti, A., 2013. Bedmap2: improved ice bed, surface and thickness datasets for Antarctica. Cryosphere 7, 375–393.

Genge, M.J., van Ginneken, M., Suttle, M.D., Harvey, R.P., 2018. Accumulation mechanisms of micrometeorites in an ancient supraglacial moraine at Larkman Nunatak, Antarctica. Meteoritics Planet Sci. 53, 2051–2066.

Geospatial Information Authority of Japan, 2014. Antarctic geospatial data. gsi.go.jp/antarctic/index-e.html.

Graly, J.A., Licht, K.J., Kassab, C.M., Bird, B.W., Kaplan, M.R., 2018. Warm-based basal sediment entrainment and far-field Pleistocene origin evidenced in central Transantarctic blue ice through stable isotopes and internal structures. J. Glaciol. 64, 185–196.

Granger, D.E., Muzikar, P.F., 2001. Dating sediment burial with in situ-produced cosmogenic nuclides: theory, techniques, and limitations. Earth Planet Sci. Lett. 188, 269–281.

Hagen, E.H., 1995. A Geochemical and Petrological Investigation of Meteorite Ablation Products in till and Ice of Antarctica (Dissertation). The Ohio State University, p. 525.

Hein, A.S., Marrero, S.M., Woodward, J., Dunning, S.A., Winter, K., Westoby, M.J., Freeman, S.P.H.T., Shanks, R.P., Sugden, D.E., 2016. Mid-Holocene pulse of thinning in the Weddell Sea sector of the West Antarctic ice sheet. Nat. Commun. 7, 12511.
Herzog, G.F., Caffee, M.W., Jull, A.J.T., 2015. Cosmogenic nuclides in antarctic meteorites. In: Righter, K., Corrigan, C., Harvey, R., McCoy, T. (Eds.), 35 Seasons of U.S. Antarctic Meteorites (1976-2010) a Pictorial Guide to the Collection. American Geophysical Union and John Wiley & Sons, Inc, pp. 153–172.
Hippe, K., 2017. Constraining processes of landscape change with combined in situ cosmogenic C-14-Be-10 analysis. Quat. Sci. Rev. 173, 1–19.
Hippe, K., Lifton, N.A., 2014. Calculating isotope ratios and nuclide concentrations for in situ cosmogenic C-14 analyses. Radiocarbon 56, 1167–1174.
Jansen, J.D., Knudsen, M.F., Andersen, J.L., Heyman, J., Egholm, D.L., 2019. Erosion rates in Fennoscandia during the past million years. Quat. Sci. Rev. 207, 37–48.
Jones, R.S., Small, D., Cahill, N., Bentley, M.J., Whitehouse, P.L., 2019. iceTEA: tools for plotting and analysing cosmogenic-nuclide surface-exposure data from former ice margins. Quat. Geochronol. 51, 72–86.
Jonsson, S., 1990. Local climate and mass balance of a blue ice area in western Dronning Maud Land, Antarctica. Z. Gletscherkd. Glazialgeol. 26, 11–29.
Kaplan, M.R., Licht, K.J., Winckler, G., Schaefer, J.M., Bader, N., Mathieson, C., Roberts, M., Kassab, C.M., Schwartz, R., Graly, J.A., 2017. Middle to late Pleistocene stability of the central East Antarctic ice sheet at the head of Law Glacier. Geology 45, 963–966.
Kassab, C.M., Licht, K.J., Petersson, R., Lindbäck, K., Graly, J.A., Kaplan, M.R., 2019. Formation and evolution of an extensive blue ice moraine in central Transantarctic Mountains, Antarctica. J. Glaciol. 66, 49–60.
Kohl, C.P., Nishiizumi, K., 1992. Chemical isolation of quartz for measurement of insitu-produced cosmogenic nuclides. Geochem. Cosmochim. Acta 56, 3583–3587.
Korotkikh, E.V., Mayewski, P.A., Handley, M.J., Sneed, S.B., Introne, D.S., Kurbatov, A.V., Dunbar, N.W., McIntosh, W.C., 2011. The last interglacial as represented in the glaciochemical record from mount moulton blue ice area, west Antarctica. Quat. Sci. Rev. 30, 1940–1947.
Korschinek, G., Bergmaier, A., Faestermann, T., Gerstmann, U.C., Knie, K., Rugel, G., Wallner, A., Dillmann, I., Dollinger, G., von Gostomski, C.L., Kossert, K., Maiti, M., Poutivtsev, M., Remmert, A., 2010. A new value for the half-life of Be-10 by Heavy-Ion Elastic Recoil Detection and liquid scintillation counting. Nucl. Instrum. Methods Phys. Res. Sect. B Beam Interact. Mater. Atoms 268, 187–191.
Kubik, P.W., Christl, M., 2010. 10Be and 26Al measurements at the Zurich 6 MV Tandem AMS facility. Nucl. Instrum. Methods Phys. Res. B 268, 880–883.
Lal, D., 1991. Cosmic-ray labeling of erosion surfaces - insitu nuclide production-rates and erosion models. Earth Planet Sci. Lett. 104, 424–439.
Lupker, M., Hippe, K., Wacker, L., Steinemann, O., Tikhomirov, D., Maden, C., Haghipour, N., Synal, H.A., 2019. In-situ cosmogenic C-14 analysis at ETH Zurich: characterization and performance of a new extraction system. Nucl. Instrum. Methods Phys. Res. Sect. B Beam Interact. Mater. Atoms 457, 30–36.
Moriwaki, K., Iwata, S., Matsuoka, N., Hasegawa, H., Hirakawa, K., 1991. Weathering stage of till and glacial history of the central Sør-Rondane Mountains. Proc. NIPR Symp. Antarct. Geosci. 5, 99–111.
Moriwaki, K., Iwata, S., Matsuoka, N., Hasegawa, H., Hirakawa, K., 1994. Weathering stage as a relative age of till in the central Sør-Rondane. Proc. NIPR Symp. Antarct. Geosci. 7, 156–161.
Mouginot, J., Rignot, E., Scheuchl, B., Millan, R., 2017. Comprehensive annual ice sheet velocity mapping using landsat-8, sentinel-1, and RADARSAT-2 data. Rem. Sens. 9, 364.
Nishiizumi, K., 2004. Preparation of Al-26 AMS standards. Nucl. Instrum. Methods Phys. Res. Sect. B Beam Interact. Mater. Atoms 223, 388–392.
Norris, T.L., Gancarz, A.J., Rokop, D.J., Thomas, K.W., 1983. Half-life of Al-26. J. Geophys. Res. 88, B331–B333.
Rignot, E., Mouginot, J., Scheuchl, B., 2017. MEaSUREs InSAR-Based Antarctica Ice Velocity Map, Version 2. Boulder, Colorado USA. NASA National Snow and Ice Data Center Distributed Active Archive Center. https://doi.org/10.5067/D7GK8F5J8M8R.
Ruff, M., Wacker, L., Gaggeler, H.W., Suter, M., Synal, H.A., Szidat, S., 2007. A gas ion source for radiocarbon measurements at 200 kV. Radiocarbon 49, 307–314.
Shakun, J.D., Carlson, A.E., 2010. A global perspective on Last Glacial Maximum to Holocene climate change. Quat. Sci. Rev. 29, 1801–1816.
Shiraishi, K., Osanai, Y., Ishizuka, H., Asami, M., 1997. Geological Map of the Sør Rondane Mountains, Antarctica. In: Antarctic Geological Map Series, Sheet, 35. National Institute of Polar Research, Tokyo. Scale 1:250000.
Sinisalo, A., Moore, J.C., 2010. Antarctic blue ice areas - towards extracting palaeoclimate information. Antarct. Sci. 22, 99–115.
Stone, J.O., 2000. Air pressure and cosmogenic isotope production. J. Geophys. Res.Solid. Earth. 105, 23753–23759.
Suganuma, Y., Miura, H., Zondervan, A., Okuno, J., 2014. East Antarctic deglaciation and the link to global cooling during the Quaternary: evidence from glacial geomorphology and Be-10 surface exposure dating of the Sor Rondane Mountains, Dronning Maud Land. Quat. Sci. Rev. 97, 102–120.
Sugden, D.E., Hein, A.S., Woodward, J., Marrero, S.M., Rodes, A., Dunning, S.A., Stuart, F.M., Freeman, S.P.H.T., Winter, K., Westoby, M.J., 2017. The million-year evolution of the glacial trimline in the southernmost Ellsworth Mountains, Antarctica. Earth Planet Sci. Lett. 469, 42–52.
Synal, H.A., Stocker, M., Suter, M., 2007. MICADAS: a new compact radiocarbon AMS system. Nucl. Instrum. Methods Phys. Res. Sect. B Beam Interact. Mater. Atoms 259, 7–13.
Tikhomirov, D., Akçar, N., Ivy-Ochs, S., Alfimov, V., Schluchter, C., 2014. Calculation of shielding factors for production of cosmogenic nuclides in fault scarps. Quat. Geochronol. 19, 181–193.
Tytgat, B., Verleyen, E., Sweetlove, M., D'hondt, S., Clercx, P., Van Ranst, E., Peeters, K., Roberts, S., Namsaraev, Z., Wilmotte, A., Vyverman, W., Willems, A., 2016. Bacterial community composition in relation to bedrock type and macrobiota in soils from the Sor Rondane Mountains, East Antarctica. FEMS Microbiol. Ecol. 92.
Wacker, L., Bonani, G., Friedrich, M., Hajdas, I., Kromer, B., Nemec, M., Ruff, M., Suter, M., Synal, H.A., Vockenhuber, C., 2010. Micadas: routine and high-precision radiocarbon dating. Radiocarbon 52, 252–262.
Whillans, I.M., Cassidy, W.A., 1983. Catch a falling star: meteorites and old ice. Science 222, 55–57.
Zekollari, H., Goderis, S., Debaille, V., van Ginneken, M., Gattacceca, J., Jull, A.J.T., Lenaerts, J.T.M., Yamaguchi, A., Huybrechts, P., Claeys, P., Aumaitre, G., Bourles, D.L., Kedadouche, K., Team, A., 2019. Unravelling the high-altitude Nansen blue ice field meteorite trap (East Antarctica) and implications for regional palaeo-conditions. Geochem. Cosmochim. Acta 248, 289–310.